THE JOURNAL OF PHYSICAL CHEMISTRY C

Article

pubs.acs.org/JPCC

Kinetic Study of the Hydrogen Oxidation Reaction on Nanostructured Iridium Electrodes in Acid Solutions

M. Angeles Montero, José L. Fernández, M. Rosa Gennero de Chialvo, and Abel C. Chialvo*

Programa de Electroquímica Aplicada e Ingeniería Electroquímica (PRELINE), Facultad de Ingeniería Química, Universidad Nacional del Litoral, Santiago del Estero 2829, 3000 Santa Fe, Argentina

ABSTRACT: The hydrogen oxidation reaction was studied on a rotating disc electrode of nanostructured iridium supported on glassy carbon. The electrode was prepared via sputtering and further annealing at 400 °C under a hydrogen atmosphere to avoid the presence of iridium oxide. The iridium film was analyzed by microscopic (scanning electron microscopy (SEM), atomic force microscopy (AFM)), spectroscopic (X-ray diffraction (XRD) and X-ray photoelectron spectroscopy (XPS)), and electrochemical (cyclic voltammetry) techniques, which allowed us to verify the nanostructured morphology and the absence of any phase other than metallic iridium. The real surface area was evaluated by adsorption of underpotential deposition (UDP) hydrogen and CO stripping. Experimental current−overpotential (η) curves of the hydrogen oxidation reaction were obtained in the range $-0.03\ \text{V} \le \eta \le 0.20\ \text{V}$ at different rotation rates in sulfuric acid solution. They were correlated by kinetic expressions, and the corresponding values of the kinetic parameters were evaluated. It was verified that over this overpotential region the reaction proceeds almost purely through the Tafel−Volmer route. Moreover, an exchange current density $j_o = 1.34\ \text{mA cm}^{-2}$ was calculated.

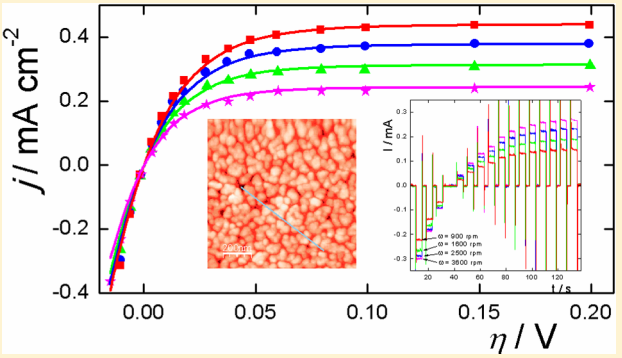

1. INTRODUCTION

Metals belonging to the platinum group (Ru, Rh, Pd, Os, Ir, and Pt) play an important role in electrochemistry, being studied as electrocatalysts for many electrode reactions.[1−4] Among them, the hydrogen electrode reaction (HER) is characterized for being the simplest electrocatalytic reaction, involving only one reaction intermediate, the adsorbed hydrogen species.[5−9] Thus, the relationship between the exchange current density (j_o) of the HER and the standard free energy of adsorption of hydrogen on the different metal surfaces could be established, resulting in the well-known volcano curve.[10−13] The elements of such groups are located on the top of the volcano plot, Pt being the most active metal.[14] These data were mainly obtained from the experimental determination of the current density (j)−overpotential (η) dependence in the cathodic range corresponding to the hydrogen evolution reaction (*her*).[15−18] On the other hand, the electrocatalytic activities of Pd[19] and Ru[20] have been determined recently from experimental measurements carried out in the anodic overpotential range, where the hydrogen oxidation reaction (*hor*) takes place. There is little information related to Ir, which is mentioned the work of J. P. Hoare and S. Schuldiner,[15] who carried out the kinetic study of the *her* and also measured the equilibrium polarization resistance (R_p^o). However, as R_p^o is a function of the inverse of the limiting diffusion current density of the molecular hydrogen (j_L),[21,22] the evaluation of R_p^o under the experimental conditions employed in that work (vigorous agitation) led to an overestimated value. Another kinetic study of the *hor* on Ir was carried out by scanning electrochemical microscopy in a perchloric acid solution.[5] The only work that studied the hydrogen oxidation in sulfuric acid solution on an Ir-rotating disc electrode was carried out by G. Bronöel and M. Haim.[23] In this case the working electrode was subjected to a pretreatment consisting of the application of 200 voltammetric cycles between 0.03 and 1.40 V vs RHE at 0.08 V s^{-1}. It is known that an oxide layer is developed during this treatment,[24−27] so that the results cannot be interpreted as the response of metallic iridium but that corresponding to a hydrated Ir oxide layer. Other results can be found in reviews related to the hydrogen electrode reaction,[12,13] where all the data were obtained from a compilation done by S. Trasatti.[14] It can be found there that the results related to Ir were obtained from two theses.[28,29] Thus, most of the information about the experimental conditions is not available.

Another aspect to be considered is that, although all the metals in the Pt group exhibit underpotential deposition of hydrogen (H_{UPD}), the electrochemical behavior is quite different. For instance, the hydrogen oxidation on Pt is verified up to high overpotentials ($\eta > 0.60$ V), before its inhibition due to the adsorption of hydroxyl species.[30] Moreover, Pd exhibits a marked capacity for hydrogen absorption, leading to the transition between the hydrides βPd−H and αPd−H, which takes place in the overpotentials region of the *hor* ($\eta \cong 0.06$

Received: August 8, 2013
Revised: September 19, 2013
Published: November 18, 2013

V).[19] Then, Ru shows a strong inhibition of the *hor* at low overpotentials (η > 0.20 V) due to its high oxyphilic properties.[20] In the case of Ir, as was already mentioned and as a different behavior to the rest of the group elements, a thick layer of hydrated oxide (Ir^{3+}, Ir^{4+}) can be easily obtained by potentiodynamic cycling, which is not reducible to metallic Ir in the working conditions.[24−27]

Therefore, taking into account the lack of experimental results related to the kinetics of the hydrogen oxidation reaction on iridium, the present work deals with the evaluation of the kinetic parameters of the Volmer−Heyrovsky−Tafel mechanism on nanostructured Ir electrodes through the correlation of experimental $j(\eta)$ curves in the overpotential range $-0.03\ \text{V} \leq \eta \leq 0.20\ \text{V}$, carried out in sulfuric acid solution under controlled mass transport conditions.

2. EXPERIMENTAL DETAILS

2.1. Electrode Preparation. The working electrodes were prepared via sputtering on a glassy carbon (GC) substrate from an iridium target (Goodfellow) in an argon atmosphere (0.1 mbar), using a sputter coater Emitech K500X, operated at 30 mA during 4 min. Previous to iridium deposition, the glassy carbon (SPI) substrate was mirror polished and subjected to ultrasonic cleaning in ultrapure water for 5 min and then was voltammetrically characterized to ensure a clean and reproducible deposition surface. Finally, the sputtered iridium electrodes were annealed in a furnace at 400 °C in a hydrogen atmosphere to avoid the presence of iridium oxide.

2.2. Electrode Characterization. The Ir/GC electrodes were physicochemically characterized by X-ray diffraction (XRD) and X-ray photoelectron spectroscopy (XPS). X-ray diffractograms were obtained with a Shimadzu XD-D1 instrument with monochromator using Cu Kα radiation at a scan rate of 2° min^{-1} in the range $20° < 2\theta < 90°$. The software package of the equipment was used for the phase identification from the diffraction peaks. The XPS measurements were carried out using a multitechnique system (SPECS) equipped with a dual Mg/Al X-ray source and a hemispherical PHOIBOS 150 analyzer operating in the fixed analyzer transmission (FAT) mode. The spectra were obtained with pass energy of 30 eV, and a Mg Ka X-ray source was operated at 200 W and 12 kV. The working pressure in the analyzing chamber was less than 5.9×10^{-7} Pa. The XPS analyses were performed in the spectral region corresponding to the Ir 4f core level.

The surface morphology of the electrodes was characterized by atomic force microscopy (AFM) and scanning electron microscopy (SEM). AFM images were obtained using a multitechnique Agilent microscope model 5400, operated in tapping mode and processed with the software WSxM 6.2. SEM micrographs were obtained with a microscope Zeiss Supra 40.

2.3. Electrochemical Measurements. All the electrochemical measurements were performed in a three-electrode cell containing 0.5 M H_2SO_4 solution at 298 K. The Ir/GC electrodes were mounted in a Teflon holder and used as working electrodes, with an exposed geometric area of 0.246 cm^2. Furthermore, a large area platinum wire acted as a counter-electrode, and the hydrogen electrode in the same solution (RHE) was used as a reference electrode. The electrodes were electrochemically characterized by cyclic voltammetry using a potentiostat-galvanostat Wenking POS2 controlled by an interface Advantech PI1710HG and the software Labview 8. The voltammograms were obtained at 0.1 V s^{-1} in nitrogen-saturated solution between 0.0 and 1.0 V.

The electrocatalytic activity of the Ir/GC electrodes toward the hydrogen oxidation reaction was evaluated through the current (I)−overpotential (η) response in hydrogen-saturated solution. The polarization curves were obtained at different rotation rates using an RDE Radiometer EDI 10k.

Finally, the real area of the electrode was determined by two experimental methods, UPD hydrogen adsorption and CO stripping voltammetry. CO adsorption was carried out in an auxiliary cell in a CO-saturated solution, holding the electrode potential at 0.05 V during 15 min. The voltammetric stripping was carried out at 0.05 V s^{-1} in nitrogen-saturated solution between 0.0 and 1.3 V.

3. RESULTS AND DISCUSSION

3.1. Morphological Characterization. Figure 1 shows a SEM micrograph that illustrates the surface morphology of the

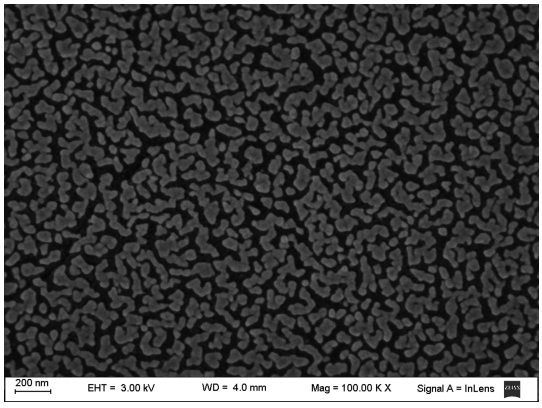

Figure 1. SEM micrograph of the nanostructured Ir/GC electrode. Magnification: 100000×.

Ir/GC electrode. It can be observed that a structure was constituted by bidimensional arrays of nanoparticles of 40 nm diameter. The Ir surface coverage was estimated from Figure 1, the resulting value being 0.65. Moreover, the image obtained by AFM is illustrated in Figure 2. From the corresponding height profile (inset in Figure 2), the average height was 40 nm, which confirms that the electrode was configured by a fraction of a monolayer with nanoparticles of 40 nm diameter agglomerated in bidimensional clusters of 5−20 particles.

3.2. Physicochemical Characterization. For the X-ray diffractogram, the sample was prepared by the application of five cycles of iridium sputtering of 4 min each, to get an adequate definition of the diffraction pattern, followed by the same thermal treatment employed for the electrodes. Figure 3 shows the XRD spectrum with diffraction peaks located at 2θ = 40.73°, 47.73°, 69.30°, and 83.65°, which are coincident to those corresponding to the Ir crystallographic planes (111), (200), (220), and (311), respectively (JCPDS-ICDD files 6-598 and 46-1044).

The result of the XPS analysis, carried out on a fresh Ir/GC electrode, is shown in Figure 4 in the range of binding energy comprised between 55 and 71 eV. Two peaks located at 61.39 and 64.48 eV, respectively, can be observed which are quite similar to the values for $4f_{7/2}$ and $4f_{5/2}$ of metal iridium (61.35 and 64.35 eV),[26] which are indicated in the figure as vertical lines. Moreover, if these values are compared to those corresponding to an IrO_x film (62.35 and 65.35 eV),[26] it can be concluded that the electrode does not exhibit an oxide film,

dx.doi.org/10.1021/jp407951u | J. Phys. Chem. C 2013, 117, 25269−25275

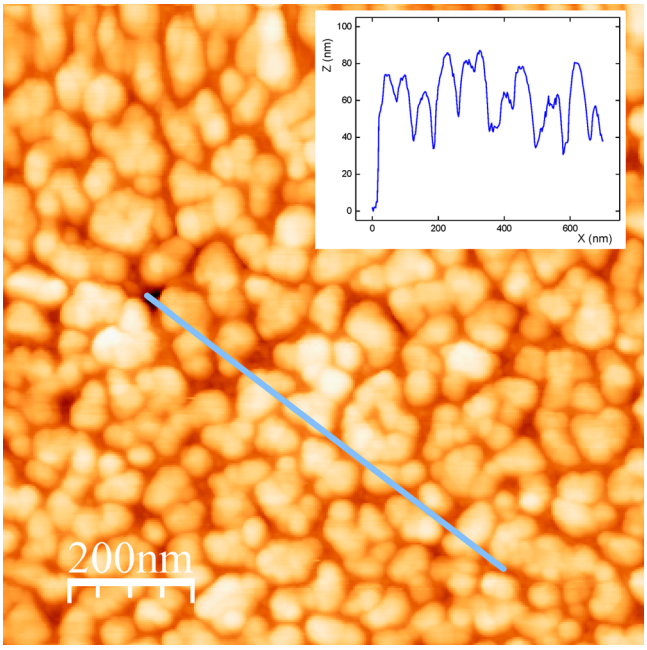

Figure 2. AFM image of the nanostructured Ir/GC electrode. Inset: height profile.

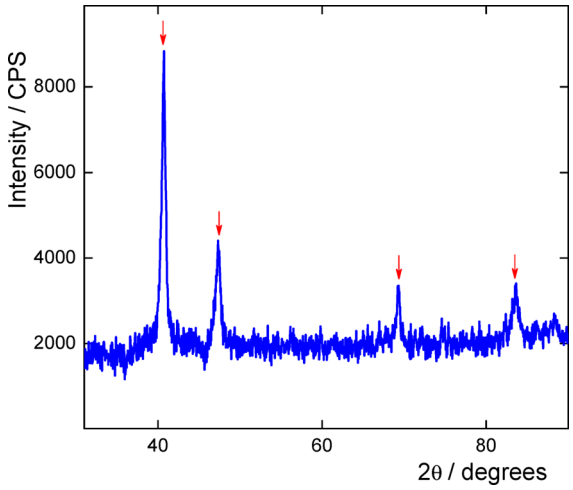

Figure 3. XRD diffractogram of the nanostructured Ir/GC electrode. Cu Kα radiation (λ = 1.5406 Å); 2° min^{-1}.

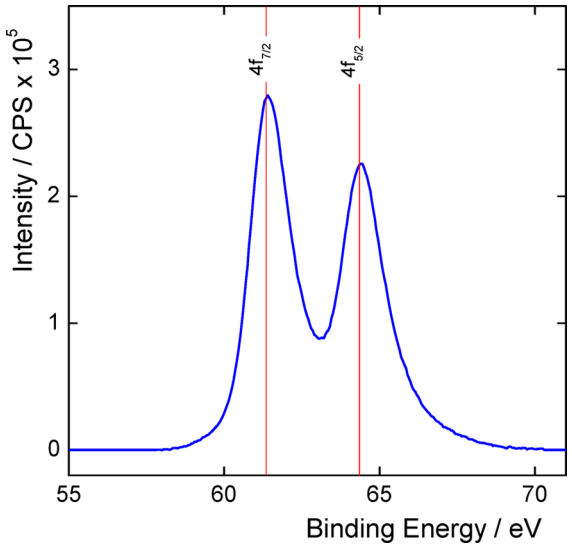

Figure 4. XPS spectra of the nanostructured Ir/GC electrode. Vertical lines indicate the values for metal Ir.[26]

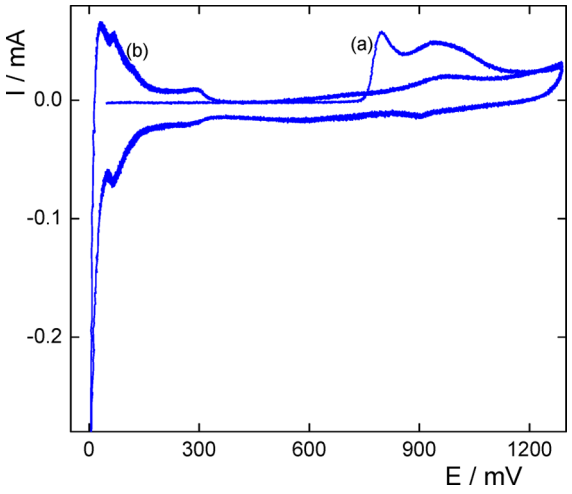

Figure 5. Voltammogram of the Ir/GC electrode after CO adsorption. (a) First cycle. (b) Second cycle. 0.05 V s^{-1}; 0.5 M H_2SO_4, 298 K.

which is in agreement with the voltammetric behavior described in the next item.

3.3. Electrochemical Characterization. Figure 5 shows the voltammetric profile of the Ir/GC electrode obtained in 0.5 M H_2SO_4 solution at 0.05 V s^{-1} corresponding to the stripping of adsorbed CO, followed by the second sweep cycle between 0.0 and 1.30 V. The complete electrooxidation of the adsorbed CO takes place in the first anodic sweep, as can be verified through the second voltammetric cycle, which reproduces the blank voltammogram of metallic iridium. It can be appreciated that the voltammetric profile, and in particular the H_{UPD} region, is quite similar to those found in the literature.[31−33] On the other hand, the voltammograms recorded to characterize the electrode previous to the kinetic measurements were obtained at 0.1 V s^{-1} between 0.0 and 1.0 V. Moreover, the electrode was not subjected to successive cycles to avoid the growth of an Ir oxide film, which is characterized by the appearance of a reversible couple at 0.95 V.[24−26]

Another important aspect is related to the relationship of the charges for the electrooxidation of adsorbed hydrogen and of CO with the real electrodic area. The first one was evaluated in the potential range comprised between 0.06 < E/V < 0.40, following the method proposed by R. Woods to estimate the electrode area.[31] The resulting value was 85.8 μC and corresponds to 65% of the charge of one monolayer of H_{UPD} (218 μC cm^{-2}). The electrode area resulting from this calculation was 0.605 cm^2. On the other hand, the charge of electrooxidation of CO was evaluated as the difference between the first and second cycle in the potential range 0.50 < E/V < 1.3, resulting in a value equal to 176.04 μC. Taking into account that for Pt[34] and for Pd[35] the CO saturation surface coverage is 66% of the adsorption sites of H_{UPD}, it should be reasonable to consider that this value can be used also for the case of Ir. Then, the charge of a CO monolayer is 287.7 μC cm^{-2}, and the corresponding value of the electrode area is 0.611 cm^2. Thus, the values of the electrode area obtained from both

dx.doi.org/10.1021/jp407951u | J. Phys. Chem. C 2013, 117, 25269−25275

the HUPD electrooxidation charge and the CO electrooxidation charge are coincident.

3.4. Hydrogen Oxidation Reaction. The evaluation of the experimental dependence of the current density on η for the hydrogen oxidation reaction started replacing nitrogen by hydrogen in the gas bubbling system of the measuring cell, while the working electrode was rotated at a given rotation rate ($900 \leq \omega/\text{rpm} \leq 3600$). A quick decrease of the open-circuit potential was produced until the equilibrium value was reached (0.0 ± 0.0003 V vs RHE). Once this condition was fulfilled, a potential program was applied, which was initiated with a 3 s step at 0.0 V, followed by a 5 s step to the desired overpotential value. In this last period, readings of the current value were made each 0.1 s, and the mean value of the current data measured in the last 2 s was assigned to the step overpotential. Then the program was repeated for each η value, which was varied in the range $-0.03 \leq \eta/\text{V} \leq 0.20$. The current ($I$)−time ($t$) response of the Ir electrode resulting from the application of the potential program is shown in Figure 6, for all the rotation

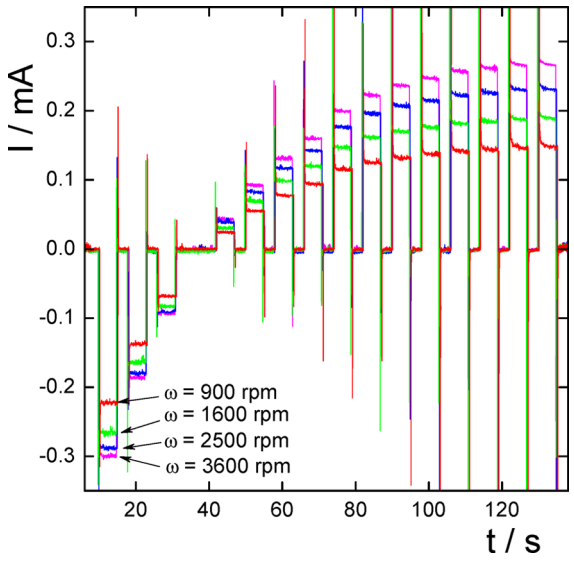

Figure 6. Current vs time response of the nanostructured Ir/GC electrode to the overpotential program applied in the range -0.03 V $\leq \eta \leq 0.20$ V at different rotation rates (indicated in the figure). 0.5 M H_2SO_4; 298 K.

rates analyzed (900, 1600, 2500, and 3600 rpm), where the stability of the electrode current on time can be verified. Starting from these results and taking into account the real electrode area, the corresponding $j(\eta)$ dependences on steady state were evaluated, which are shown in Figure 7 (symbols). These experimental curves were correlated with a system of equations described in the following item.

3.5. Mechanistic Description of the Hydrogen Oxidation on Ir. It is generally accepted that the hydrogen electrode reaction on a metallic surface is verified through the elementary steps of Tafel, Heyrovsky, and Volmer

$$H_2 + 2S \rightleftarrows 2H_{ad} \quad \text{Tafel} \tag{1-1}$$

$$H_2 + S \rightleftarrows H_{ad} + H^+ + e^- \quad \text{Heyrovsky} \tag{1-2}$$

$$H_{ad} \rightleftarrows H^+ + e^- + S \quad \text{Volmer} \tag{1-3}$$

where S represents a site on the electrode surface in which the reaction intermediate H_{ad} can be adsorbed. The resolution of

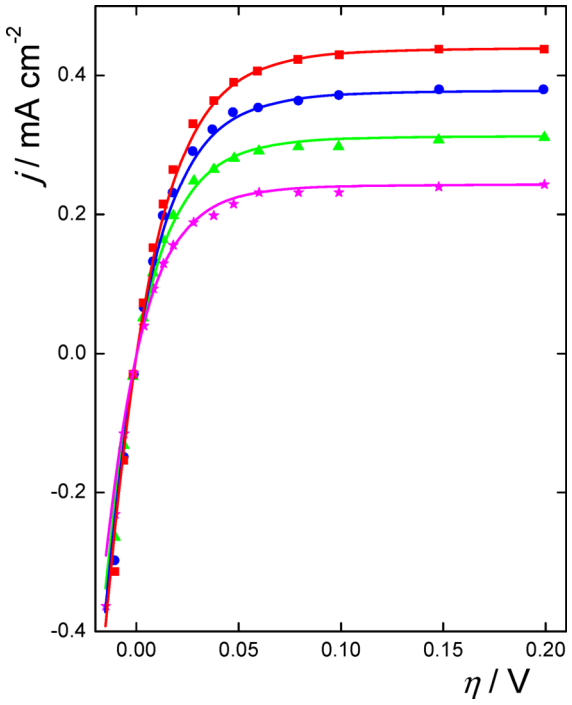

Figure 7. Experimental (symbols) and simulated (lines) $j(\eta)$ curves of the *hor* on the nanostructured Ir/GC electrode. 0.5 M H_2SO_4; 298 K. ω = (★) 900; (▲) 1600; (●) 2500; (■) 3600.

the kinetic mechanism of Tafel−Heyrovsky−Volmer implies that the hydrogen oxidation is verified under the simultaneous occurrence of both Tafel−Volmer and Heyrovsky−Volmer routes, and it considers a Frumkin type adsorption for the reaction intermediate.[9] It also takes into account an active area factor (f_{aa}), which takes into account the relationship between the area where the reaction takes place (real area) and that corresponding to the diffusion flux of molecular hydrogen (geometric area).[36] This number acts as a correction factor of the limiting diffusion current density (j_L), which is related to the geometric area and for the case of a rotating disc electrode is equal to $j_L = B\omega^{1/2}$.[37] Although three equivalent expressions for $j(\eta)$ can be derived, referring to the real or active area, the equation used in the present work was[38]

$$j = \left\{ \nu_H^e e^{-u(\theta-\theta^e)\lambda} e^{\alpha_H f\eta} \left[\frac{(1-\theta)}{(1-\theta^e)} - \frac{\theta e^{-f\eta} e^{u(\theta-\theta^e)}}{\theta^e} \right] + \nu_T^e e^{-2u(\theta-\theta^e)\lambda} \left[\frac{(1-\theta)^2}{(1-\theta^e)^2} - \frac{\theta^2 e^{2u(\theta-\theta^e)}}{\theta^{e^2}} \right] \right\} / \left\{ \frac{1}{2F} + \frac{\nu_T^e f_{aa} (1-\theta)^2 e^{-2u(\theta-\theta^e)\lambda}}{B\omega^{1/2}(1-\theta^e)^2} + \frac{\nu_H^e f_{aa} (1-\theta) e^{-u(\theta-\theta^e)\lambda} e^{\alpha_H f\eta}}{B\omega^{1/2}(1-\theta^e)} \right\} \tag{2}$$

The implicit equation for the variation of the surface coverage (θ) of the reaction intermediate on overpotential is given by[38]

dx.doi.org/10.1021/jp407951u | J. Phys. Chem. C 2013, 117, 25269−25275

$$\left\{ v_V^e e^{-u(\theta-\theta^e)\lambda} e^{\alpha_V f\eta}\left[\frac{\theta e^{u(\theta-\theta^e)}}{\theta^e} - \frac{(1-\theta)e^{-f\eta}}{(1-\theta^e)}\right] + v_H^e e^{-u(\theta-\theta^e)\lambda} e^{\alpha_H f\eta}\left[\frac{(1-\theta)}{(1-\theta^e)} - \frac{\theta e^{-f\eta} e^{u(\theta-\theta^e)}}{\theta^e}\right]\right\} \times \left\{\frac{1}{2F} + \frac{v_T^e f_{aa}(1-\theta)^2 e^{-2u(\theta-\theta^e)\lambda}}{B\omega^{1/2}(1-\theta^e)^2}\right\} - \left\{\frac{1}{F} + \frac{v_H^e f_{aa}(1-\theta)e^{-u(\theta-\theta^e)\lambda} e^{\alpha_H f\eta}}{B\omega^{1/2}(1-\theta^e)}\right\} \times \left\{ v_V^e e^{-u(\theta-\theta^e)\lambda} e^{\alpha_V f\eta}\left[\frac{\theta e^{u(\theta-\theta^e)}}{\theta^e} - \frac{(1-\theta)e^{-f\eta}}{(1-\theta^e)}\right] - v_T^e e^{-2u(\theta-\theta^e)\lambda}\left[\frac{(1-\theta)^2}{(1-\theta^e)^2} - \frac{\theta^2 e^{2u(\theta-\theta^e)}}{\theta^{e^2}}\right]\right\} = 0 \quad (3)$$

where v_i is the reaction rate of the step i (i = T, H, V); α_i (i = V,H) is the symmetry factor of the step i; λ is the symmetry factor of adsorption; and u (in RT units) is the energy of interaction between the adsorbed hydrogen atoms. Superscript e indicates equilibrium, and $f = F/RT$.

By the use of eqs 2 and 3, the experimental dependence $j(\eta)$ on steady state measured at a given rotation rate can be correlated, and the corresponding set of kinetic parameters can be evaluated. However, it is necessary first to evaluate the value of the relationship f_{aa}/B. This constant can be evaluated from the values of the maximum current (j_{max}) observed for $\eta > 0.15$ V, as it is related to the rotation rate as follows[9]

$$\frac{1}{j_{max}(\omega)} = \frac{1}{j_{max}^{kin}} + \left(\frac{f_{aa}}{B}\right)\frac{1}{\omega^{1/2}} \quad (4)$$

where j_{max}^{kin} is the limiting kinetic current density of the Tafel step. Equation 4 highlights the mixed behavior of the hydrogen oxidation, with simultaneous kinetic and diffusion contributions. j_{max}^{kin} is originated when the potential increase causes the hydrogen surface coverage to vanish before the surface concentration of molecular hydrogen goes to zero, and it is given by the following expression[9]

$$j_{max}^{kin} = \frac{2Fv_T^e e^{2\lambda u\theta^e}}{(1-\theta^e)^2} \quad (5)$$

Thus, the slope of the experimental plot j_{max}^{-1} vs $\omega^{-1/2}$ gives the constant f_{aa}/B, and the corresponding value of the origin ordinate is equal to the inverse of j_{max}^{kin}. Figure 8 illustrates such a plot, where it can be observed that the experimental points satisfy the required linearity.

The linear regression gives the following values: f_{aa}/B = 110.5424 mA^{-1} cm^2 rpm$^{1/2}$ and $(j_{max}^{kin})^{-1}$ = 0.43637 mA^{-1} cm^2. Moreover, eq 5 imposes a relationship between the equilibrium reaction rate of the Tafel step (v_T^e) and the equilibrium surface coverage (θ^e), which for the present case is

$$v_T^e\ [\text{mol cm}^{-2}\ \text{s}^{-1}] = 1.187510^{-8}(1-\theta^e)^2 e^{-2u\theta^e} \quad (6)$$

Then, the experimental $j(\eta)$ curves were correlated using eqs 2, 3, and 6, applying a nonlinear least-squares regression method. This calculation was carried out with the software Micromath Scientific 3.0, considering the symmetry factors $\alpha_V = \alpha_H = \lambda$ = 0.5. Thus, only the kinetic parameters v_V^e, v_H^e, θ^e, and u were evaluated from the correlation. Then, the value of v_T^e was obtained from eq 6. Each polarization curve corresponding to a particular rotation rate was correlated independently. The mean value of each kinetic parameter and the corresponding standard deviation are shown in Table 1.

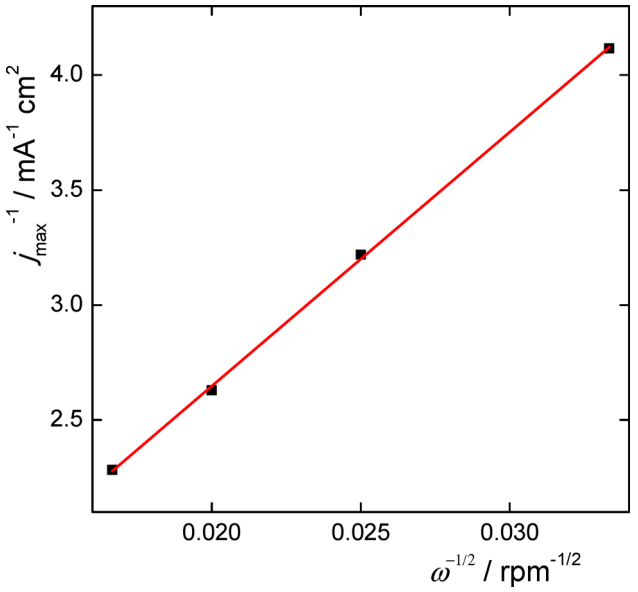

Figure 8. j_{max}^{-1} vs $\omega^{-1/2}$ plot. Experimental (symbols), linear regression (line).

Table 1. Kinetic Parameters for the *hor* from the Correlation of Experimental Results

kinetic parameters	
v_V^e/mol cm^{-2} s^{-1}	9.89 ± 2.65 × 10^{-5}
v_H^e/mol cm^{-2} s^{-1}	<10^{-15}
v_T^e/mol cm^{-2} s^{-1}	6.92 ± 1.12 × 10^{-9}
θ^e	0.459 ± 0.05
u/RT	0.75 ± 0.01

Moreover, the simulations of the dependencies $j(\eta)$ at each rotation rate were done with this unique set of parameters, which are shown in Figure 7 (lines). It can be appreciated that there is a good agreement between the experimental and simulated curves and that in the analyzed potential range the hydrogen oxidation is verified through the Tafel-Volmer route, the contribution of the Heyrovsky–Volmer route being negligible.

3.6. Electrocatalytic Activity. As it has already been mentioned, in the volcano plot the electrocatalytic activity is represented by the exchange current density (j^o). The rigorous relationship of j^o with the equilibrium reaction rates of the Tafel, Heyrovsky, and Volmer steps is given by[39]

$$j^o = 2F\left(\frac{v_T^e v_V^e + v_H^e v_V^e + v_T^e v_H^e}{(v_V^e + v_H^e + 2v_T^e)}\right) \quad (7)$$

Therefore, the value obtained from the data given in Table 1 is j^o = 1.34 mA cm^{-2}, which is slightly higher than that mentioned in the literature (0.251 mA cm^{-2}).[14] On the other hand, the value calculated for platinum nanoparticles supported on GC (data taken from Table 1, Electrode F)[40] is j^o = 45.9 mA cm^{-2}, much higher than the value obtained for the exchange current density of the hydrogen electrode reaction on Ir.

dx.doi.org/10.1021/jp407951u | J. Phys. Chem. C 2013, 117, 25269–25275

On the other hand, the values of the equilibrium polarization resistance (R_p^o) can also be compared, and the relationship with the kinetic parameters is given by[39]

$$R_p^o = \frac{RT}{4F^2}\left(\frac{4\nu_T^e + \nu_H^e + \nu_V^e}{\nu_T^e\nu_V^e + \nu_H^e\nu_V^e + \nu_T^e\nu_H^e}\right) \quad (8)$$

The value R_p^o = 9.62 Ω cm^2 was calculated on Ir, which is lower than that reported by J. P. Hoare and S. Schuldiner (18.8 Ω cm^2).[15] As expected, it is also significantly higher than that on Pt (0.355 Ω cm^2).[40]

4. CONCLUSIONS

The hydrogen oxidation reaction was studied on a rotating disc electrode of nanostructured iridium supported on glassy carbon, free of hydrated Ir oxide. The electroactive area was evaluated by CO stripping, and the value obtained is in agreement with that calculated from the voltammetric charge of H_{UPD} electroadsorption. The correlation of the experimental current−potential curves allowed the evaluation of the kinetic parameters of the Tafel−Heyrovsky−Volmer mechanism. It was demonstrated that in the analyzed overpotential region the reaction takes place through the Tafel−Volmer route. Finally, self-consistent values of the exchange current density and the equilibrium polarization resistance of the hydrogen electrode reaction were evaluated from the results obtained. These results were compared with values reported in the literature. The importance of appropriate conditions for the diffusion of molecular hydrogen during the experimental evaluation of the kinetic constants is evidenced.

AUTHOR INFORMATION

Corresponding Author

*Tel.: +54 342 457 1164 2519. E-mail: achialvo@fiq.unl.edu.ar.

Notes

The authors declare no competing financial interest.

ACKNOWLEDGMENTS

The authors wish to acknowledge the financial support received from ANPCyT, CONICET, and UNL. Thanks are also given to ANPCyT for the purchase of the SPECS multitechnique analysis instrument (PME8-2003).

REFERENCES

(1) Zhao, J.; Zhang, L.; Chen, T.; Yu, H.; Zhang, L.; Xue, H.; Hu, H. Supercritical Carbon-Dioxide-Assisted Deposition of Pt Nanoparticles on Graphene Sheets and Their Application as an Electrocatalyst for Direct Methanol Fuel Cells. *J. Phys. Chem. C* **2012**, *116*, 21374−21381.

(2) Shao, M.; Odell, J.; Humbert, M.; Yu, T.; Xia, Y. Electrocatalysis on Shape-Controlled Palladium Nanocrystals: Oxygen Reduction Reaction and Formic Acid Oxidation. *J. Phys. Chem. C* **2013**, *117*, 4172−4180.

(3) Rau, M. S.; Gennero de Chialvo, M. R.; Chialvo, A. C. Effect of the Pt/Ru Intermetallic Boundary on the Carbon Monoxide Electrooxidation: Excess Electrocatalytic Activity. *J. Power Sources* **2012**, *216*, 464−470.

(4) Ortiz, R.; Marquez, O. P.; Marquez, J.; Gutierrez, C. Necessity of Oxygenated Surface Species for the Electrooxidation of Methanol on Iridium. *J. Phys. Chem.* **1996**, *100*, 8389−8396.

(5) Zoski, C. G. Scanning Electrochemical Microscopy: Investigation of Hydrogen Oxidation at Polycrystalline Noble Metal Electrodes. *J. Phys. Chem. B* **2003**, *107*, 6401−6405.

(6) Santana, J. A.; Mateo, J. J.; Ishikawa, I. Electrochemical Hydrogen Oxidation on Pt(110): A Combined Direct Molecular Dynamics/Density Functional Theory Study. *J. Phys. Chem. C* **2010**, *114*, 4995−5002.

(7) Santos, E.; Lundin, A.; Potting, K.; Quaino, P.; Schmickler, W. Model for the electrocatalysis of hydrogen evolution. *Phys. Rev. B* **2009**, *79*, 235436.

(8) Hoshi, N.; Asaumi, Y.; Nakamura, M.; Mikita, K.; Kajiwara, R. Structural Effects on the Hydrogen Oxidation Reaction on n(111)−(111) Surfaces of Platinum. *J. Phys. Chem. C* **2009**, *113*, 16843−16846.

(9) Gennero de Chialvo, M. R.; Chialvo, A. C. Hydrogen Diffusion Effects on the Kinetics of the Hydrogen Electrode Reaction. Part I. Theoretical Aspects. *Phys. Chem. Chem. Phys.* **2004**, *6*, 4009−4017.

(10) Parsons, R. The Rate of Electrolytic Hydrogen Evolution and the Heat of Adsorption of Hydrogen. *Trans. Faraday Soc.* **1958**, *54*, 1053−1063.

(11) Saraby-Reintjes, A. Electrocatalysis under Temkin Adsorption Conditions. *J. Chem. Soc., Faraday Trans. I* **1987**, *83*, 271−279.

(12) Petrii, O. A.; Tsirlina, G. A. Electrocatalytic Activity Prediction for Hydrogen Electrode Reaction: Intuition, Art, Science. *Electrochim. Acta* **1994**, *39*, 1739−1747.

(13) Norskov, J. K.; Bligaard, T.; Logodottir, A.; Chen, J. G.; Pandelov, S.; Stimming, U. Trends in the Exchange Current for Hydrogen Evolution. *J. Electrochem. Soc.* **2005**, *152*, J23−J26.

(14) Trassati, S. Work Function, Electronegativity, and Electrochemical Behaviour of Metals. III. Electrolytic Hydrogen Evolution in Acid Solutions. *J. Electroanal. Chem.* **1972**, *39*, 163−184.

(15) Hoare, J. P.; Schuldiner, S. Hydrogen Overvoltage on Bright Iridium and Rhodium. *J. Chem. Phys.* **1956**, *25*, 786.

(16) Bockris, J. O'M.; Srinivasan, S. Elucidation of the Mechanism of Electrolytic Hydrogen Evolution by the Use of H-T Separation Factors. *Electrochim. Acta* **1964**, *9*, 31−44.

(17) Wrona, P. K.; Lasia, A.; Lessard, M.; Menard, H. Kinetics of the Hydrogen Evolution Reaction on a Rhodium Electrode. *Electrochim. Acta* **1992**, *37*, 1283−1294.

(18) Horvat-Radosevic, V.; Kvastek, K. Some Aspects of the EIS Study of the Rhodium Electrode in the Hydrogen Evolution Region. *Electrochim. Acta* **2002**, *48*, 311−322.

(19) Rau, M. S.; Quaino, P. M.; Gennero de Chialvo, M. R.; Chialvo, A. C. Hydrogen Oxidation Reaction: Evidences of Different Electrocatalytic Activity between α and β Pd-H. *Electrochem. Commun.* **2008**, *10*, 208−212.

(20) Rau, M. S.; Gennero de Chialvo, M. R.; Chialvo, A. C. A Feasible Kinetic Model for the Hydrogen Oxidation on Ruthenium Electrodes. *Electrochim. Acta* **2010**, *55*, 5014−5018.

(21) Bagotzky, V. S.; Osetrova, N. V. Investigation of Hydrogen Ionization on Platinum with the Help of Micro-Electrodes. *J. Electroanal. Chem.* **1973**, *43*, 233−249.

(22) Quaino, P. M.; Gennero de Chialvo, M. R.; Chialvo, A. C. Hydrogen Diffusion Effects on the Kinetics of the Hydrogen Electrode Reaction. Part II. Evaluation of Kinetics Parameters. *Phys. Chem. Chem. Phys.* **2004**, *6*, 4450−4455.

(23) Bronöel, G.; Haim, M. Hydrogen Oxidation-Reduction on Platinum and Iridium Electrodes. *J. Chim. Phys.* **1976**, *73*, 952−960.

(24) Gottesfeld, S.; McIntyre, J. D. E. Electrochromism in Anodic Iridium Oxide Films. II. pH Effects on Corrosion Stability and the Mechanism of Coloration and Bleaching. *J. Electrochem. Soc.* **1979**, *126*, 742−750.

(25) Lezna, R. O.; de Tacconi, N. R.; Arvia, J. A. The Electrochemical Behaviour of Iridium/Silver Loaded Iridium Oxide Electrodes in Acid Electrolytes. *J. Electroanal. Chem.* **1985**, *18*, 109−117.

(26) El Sawy, E. N.; Birss, V. I. Nano-Porous Iridium and Iridium Oxide Thin Films Formed by High Efficiency Electrodeposition. *J. Mater. Chem.* **2009**, *19*, 8244−8252.

(27) Augustynki, J.; Koudelka, M.; Sanchez, J.; Conway, B. E. ESCA Study of the State of Iridium and Oxygen in Electrochemically and Thermally Formed Iridium Oxide Films. *J. Electroanal. Chem.* **1984**, *160*, 233−248.

(28) Matthews, D. B. *PhD Thesis*, University of Pennsylvania, 1965.

(29) Mannan, R. J. *PhD Thesis*, University of Pennsylvania, 1967.

(30) Rau, M. S.; Gennero de Chialvo, M. R.; Chialvo, A. C. Kinetic study of the hydrogen oxidation reaction on Pt over the complete overpotential range. *J. Power Sources* **2013**, *229*, 210−215.
(31) Woods, R. Hydrogen Adsorption on Platinum, Iridium and Rhodium Electrodes at Reduced Temperatures and the Determination of Real Surface Area. *J. Electroanal. Chem.* **1974**, *49*, 217−226.
(32) Mozota, J.; Conway, B. E. Surface and Bulk Processes at Oxidized Iridium Electrodes. I. Monolayer Stage and Transition to Reversible Multilayer Oxide Film Behaviour. *Electrochim. Acta* **1983**, *28*, 1−8.
(33) Aramata, A.; Yamazaki, T.; Kunimatsu, K.; Enyo, M. Electrooxidation of Methanol on Iridium in Acidic Solutions: Electrocatalysis and Surface Characterization by Infrared Spectroscopy. *J. Phys. Chem.* **1987**, *91*, 2309−2314.
(34) Offer, G. J.; Kucernak, A. R. Calculating the Coverage of Saturated and Sub-Saturated Layers of Carbon Monoxide Adsorbed onto Platinum. *J. Electroanal. Chem.* **2008**, *613*, 171−185.
(35) Fang, L.; Tao, Q.; Li, M.; Liao, L.; Chen, D.; Chen, Y. Determination of the Real Surface Area of Palladium Electrode. *Chin. J. Phys. Chem.* **2010**, *23*, 543−548.
(36) Montero, M. A.; Gennero de Chialvo, M. R.; Chialvo, A. C. Rotating Nanoparticle Array Electrode for the Kinetics Study of Reactions Under Mixed Control. *Electrochim. Acta* **2010**, *56*, 756−761.
(37) Levich, V. G. *Physicochemical Hydrodynamics*; Prentice-Hall: Englewood Cliffs, NJ, 1962.
(38) Montero, M. A.; Gennero de Chialvo, M. R.; Chialvo, A. C. Electrocatalytic Activity of Core-Shell Au@Pt Nanoparticles for the Hydrogen Oxidation Reaction. *Int. J. Hydrogen Energy* **2011**, *36*, 3811−3816.
(39) Gennero de Chialvo, M. R.; Chialvo, A. C. Existence of Two Sets of Kinetic Parameters in the Correlation of the Hydrogen Electrode Reaction. *J. Electrochem. Soc.* **2000**, *147*, 1619−1622.
(40) Montero, M. A.; Gennero de Chialvo, M. R.; Chialvo, A. C. Hydrogen oxidation reaction on platinum nanoparticles: Transition between mechanistic routes. *Electrochem. Commun.* **2010**, *12*, 398−401.